small methods
www.small-methods.com

Single-Molecule Electrical Detection with Real-Time Label-Free Capability and Ultrasensitivity

*Chunhui Gu, Chuancheng Jia, and Xuefeng Guo**

Single-molecule detection based on electricity can realize direct, real-time, and label-free monitoring of the dynamic processes of either chemical reactions or biological functions at the single-molecule/single-event level. This provides a fascinating platform to probe detailed information of chemical and biological reactions, including intermediates/transient states and stochastic processes that are usually hidden in ensemble-averaged experiments, which is of crucial importance to chemical, biological, and medical sciences. Here, the focus is on a valuable survey of the state-of-art progress in single-molecule dynamics studies that are based on electrical nanocircuits formed from one-dimensional nanoarchitectures and molecular-tunneling junctions. Further interesting applications, useful statistical-analysis methods, and future promising directions toward the study of chemical-reaction dynamics and biomolecular activities are also discussed.

1. Introduction

The dynamics of molecular reactions are central scientific problems in both chemistry and biology.[1] Real-time monitoring of intermediates/transition states and time-dependent pathways of reaction dynamics is crucial for obtaining fundamental understanding of the intrinsic mechanisms. Measurements at the macroscopic level yield ensemble-averaged reaction dynamics, while investigations at the microscopic level reveal more detailed information at the molecular level. Therefore, single-molecule detection has obvious advantages for molecular recognition and examination of reaction dynamics.

Single-molecule techniques can transduce intrinsic characteristics, such as conformational changes and molecular interactions, into detectable optical, mechanical, or electrical signals. These signals are correlated with specific molecular states and provide rich information concerning intermediates/transient states and stochastic processes of the reactions.[2,3] Therefore, this unique real-time monitoring provides detailed dynamics that are hidden in ensemble-average experiments, which is important to reveal the reaction mechanisms. In addition, by detecting trace amounts of analytes, single-molecule techniques can also be used for molecular recognition[4] of small molecules and nonreplicated characteristics of bio-macromolecules, such as DNA methylation[5] or protein phosphorylation and glycosylation.[6]

In this regard, various single-molecule detection platforms have been built. Among these approaches, electrical platforms based on nanoscale circuits are particularly attractive because of their remarkable advantages including real-time measurement, label-free ability, high time resolution, and potential integration capability. In these electrical platforms, without the requirements of fluorescent labeling or an external reference standard, the intrinsic properties of individual molecules and their responses to the surrounding environments can be directly monitored. These advantages distinguish electrical devices as unique platforms for in situ investigations of chemical reactions and biological interactions at the single-molecule/single-event level. In particular, these methods enable us to study stochastic fluctuations under equilibrium conditions and reveal time trajectories and reaction pathways of individual species in non-equilibrated systems, which is of fundamental importance in elucidating traditionally indecipherable reaction mechanisms. Furthermore, these devices are promising to serve as local reporters for sensing individual binding events in biological systems, such as DNA hybridization, genetic mutation, or molecular diagnostics. Here, we aim to summarize the significant advances of single-molecule electronic techniques developed recently and highlight their importance and great potential of further applications in reaction dynamics and molecular recognition.

2. From Single-Molecule Optics to Single-Molecule Electronics

Optical (fluorescence) methods have enabled considerable advances in single-molecule recognition and reaction dynamics. Fluorescence correlation spectroscopy (FCS) was one of the first techniques for studying single-molecule dynamics.[7,8] In FCS, target molecules are usually labeled with a fluorophore

C. Gu, Dr. C. Jia, Prof. X. Guo
Beijing National Laboratory for Molecular Sciences
State Key Laboratory for Structural Chemistry
of Unstable and Stable Species
College of Chemistry and Molecular Engineering
Peking University
Beijing 100871, P. R. China
E-mail: guoxf@pku.edu.cn
Prof. X. Guo
Department of Materials Science and Engineering
College of Engineering
Peking University
Beijing 100871, P. R. China

DOI: 10.1002/smtd.201700071

and a quencher (**Figure 1**a). The concentration of target molecules must be diluted enough to guarantee that only one molecule transits the beam waist at any one time. The folding processes can be detected when the fluorophore approaches the quencher, resulting in quenched emission. FCS has a time resolution of nanoseconds. However, due to Brownian motion, continuous monitoring of a target molecule usually lasts less than 100 µs. To achieve long time measurement, immobilization methods that utilize single-molecule Förster resonance energy transfer (smFRET) have been developed (Figure 1b).[3,9] For example, the target molecule can be immobilized on a substrate via a biotin–streptavidin linkage. The target molecule is labeled at key sites with donor and acceptor dyes that are designed for spectral analysis. The donor nonradiatively transfers the excitation energy to the acceptor, which leads to fluorescence quenching of the donor and emission from the acceptor. Because the energy-transfer efficiency is highly sensitive to the inter-dye distance, millisecond conformational changes in the target molecule can be detected from the fluorescence signals. Single-molecule fluorescence can be combined with a real-time optical monitoring platform. For example, the combination with nanoscale zero-mode waveguide arrays enables parallel volume confinement for optical observation. In this way, thousands of single-DNA-sequencing steps can be monitored simultaneously (Figure 1c).[10] In detail, different deoxyribonucleoside triphosphate (dNTPs) molecules are labeled with corresponding fluorophores. When the dNTPs bond with single immobilized polymerase molecules according to the sequence of the target template, each dNTP during DNA synthesis can be identified via the fluorescence wavelength, thus realizing real-time DNA sequencing.

As discussed above, optical methods are generally based on the fluorescent changes, which usually requires fluorescent labeling. The commonly used fluorescent agents include organic fluorophores, fluorescent proteins, and semiconductor quantum dots, each of which might have problems of size effects, photobleaching, blinking, and low labeling efficiency. In addition, the timescale from 100 µs to 10 ms, during which the most important biochemical processes usually occur, is the vacuum of the main optical methods including FCS and smFRET. In comparison with optical approaches, electronic techniques for single-molecule detection avoid problems of fluorescence labeling,[11,12] have a wider detection time that can correlate with biochemical reactions,[13] and can be used to investigate small molecules. For example, methods based on ionic conductivity were the first to detect single molecules. Membrane nanopores, including biological[14,15] and artificial nanopores,[16–18] are widely used in molecular recognition[19] and label-free DNA sequencing.[20,21] In this case, a transmembrane potential is applied on both sides of the nanopore, inducing a stable ion current through the pore. When the nanopore is blocked by a target molecule, a temporary current blockade is detected (Figure 1d). Features of the molecular units in the nanopores, such as DNA bases, can be deduced from the current blockade. Nanopores can also be decorated with various recognition sites that are selective to specific analytes, such as metal ions and organic compounds. Considering the major theme here with the limited space, we are not able to cover all the aspects of nanopore ionic current-based methods.

Chunhui Gu received his B.S. degree in 2014 from the College of Chemistry and Molecular Engineering, Peking University, Beijing. He is currently working toward a Ph.D. degree in chemistry at the College of Chemistry and Molecular Engineering, Peking University, under the guidance of Prof. Xuefeng Guo. His current research interests include single-molecule devices and dynamics.

Chuancheng Jia is currently a postdoctoral researcher in the College of Chemistry and Molecular Engineering, Peking University, and the Institute of Chemistry, Chinese Academy of Sciences, under the guidance of Prof. Xuefeng Guo and Prof. Daoben Zhu. He received his Ph.D. degree in 2014 from the College of Chemistry and Molecular Engineering, Peking University, under the guidance of Prof. Xuefeng Guo. His research is focused on single-molecule devices and dynamics.

Xuefeng Guo received his Ph.D. in 2004 from the Institute of Chemistry, Chinese Academy of Sciences, Beijing. From 2004 to 2007, he was a postdoctoral research scientist at the Columbia University Nanocenter. He joined the faculty as a professor under the "Peking 100-Talent" Program at Peking University in 2008. His current research is focused on functional nanometer/molecular devices.

For an advanced technical overview in this field, readers can refer to recent comprehensive reviews.[22–24] Another example of molecular detection via ionic conductivity is an electrochemical approach,[25] such as the detection of individual redox-active molecules that are amplified via rapid redox circulation between electrodes (Figure 1e). Ionic-conductivity methods usually have disadvantages such as being complicated processes, showing low widespread applicability, and having restricted analytes.

The electrical platforms discussed in this article operate via electron conduction. These transistor-like platforms have

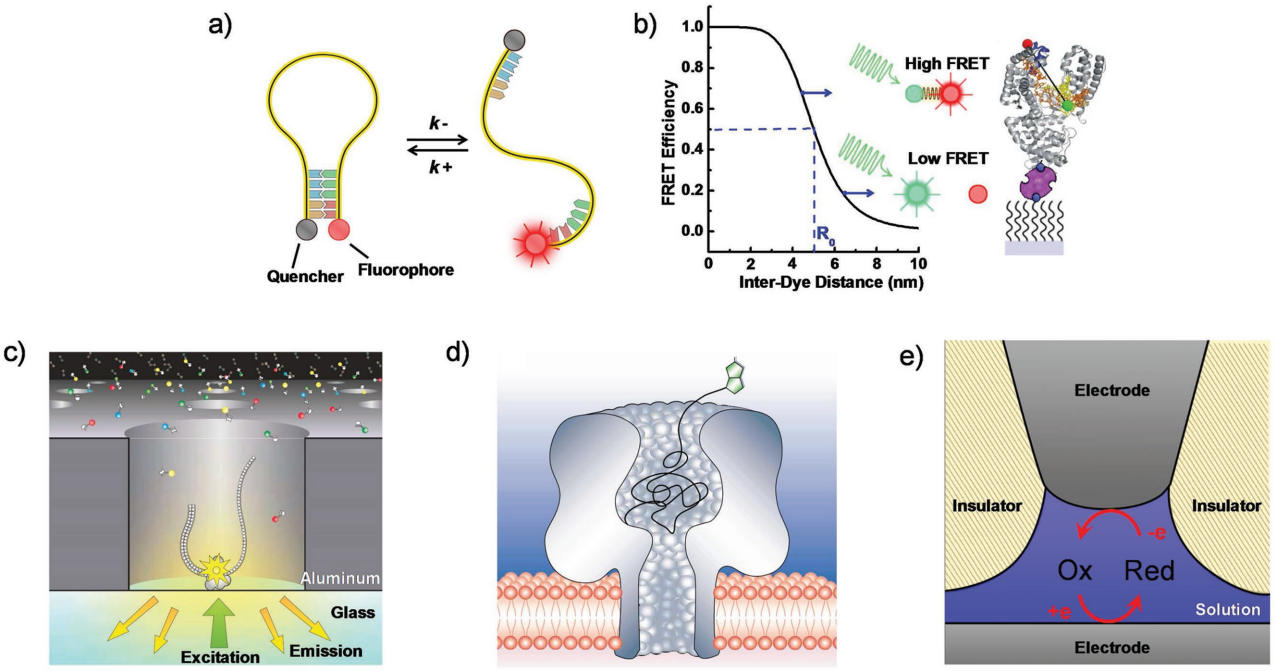

Figure 1. Single-molecule detection techniques. a) FRET detection of closed and open states for DNA that is labeled with a fluorophore and a quencher. b) FRET efficiency vs distance between a donor and an acceptor, where a short distance leads to efficient FRET and a long distance leads to low FRET. The right side depicts an oligonucleotide labeled with donor and acceptor dyes and is immobilized on a substrate via a biotin–streptavidin linkage. c) Single-DNA sequencing via fluorescence detection in a zero-mode waveguide nano-array. d) Nanopores for single-molecule sensing via ion-current blockages. e) Electrochemical single-molecule detection that depends on rapid circulation of redox-active molecules. a) Reproduced with permission.[7] Copyright 1998, National Academy of Sciences. b,left) Adapted with permission.[9] Copyright 2008, Nature Publishing Group. b,right) Adapted with permission.[3] Copyright 2012, American Chemical Society. c) Reproduced with permission.[10] Copyright 2009, American Association for the Advancement of Science. d) Reproduced with permission.[19] Copyright 2001, Nature Publishing Group. e) Reproduced with permission.[25] Copyright 1995, American Association for the Advancement of Science.

advantages as noted above. In addition, they have a faster response speed relative to ionic conduction. Mature immobilization techniques enable longer continuous measurements on one particular molecule. Such unique single-molecule electrical platforms determine that only individual molecules involved in the circuit can be detected, which makes single-molecule detection possible even when the analyte is not highly diluted. Finally, solid-state fabrication of chip-shaped devices has the potential for integration and in vivo applications.

3. One-Dimensional Nanotransistors for Single-Molecule Detection

Single-molecule detection involves the transduction of molecular properties into detectable signals, such as tracking diffusion via fluorescence. Quasi one-dimensional nanomaterials, such as nanowires, nanotubes, and atomically thin nanoribbons have cross-sections that are of the same scale as molecules (especially biomolecules). When a target molecule interacts with a one-dimensional (1D) nanoscale field-effect transistor (FET), the intrinsic charge distribution on the molecule could affect conduction through the field effect. Thus, electrical signals from the FET can be used to detect the molecule.

3.1. Nanowire Platforms

Semiconductor nanowires have been used as biosensors for single cells and also for single molecules. For example, a silicon-nanowire FET device can detect, via charge scattering, the interaction between an antibody and the influenza virus at the single-molecule level.[26] When combined with high-speed data acquisition, the device could be a real-time single-molecule detector.

Silicon nanowires confirm that nanopore–nanowire devices can sense single molecules at a high sampling rate.[27] The sensor is a silicon nanowire, formed via chemical vapor deposition (CVD), on which a single solid-state nanopore is fabricated. It has two operating modes; namely, ionic conductance through the nanopore and electronic conductance through the nanowire (**Figure 2**a). When double-stranded DNA passes through the nanopore, the ionic conductance is blocked. At the same time, the nanowire FET conductance decreases because of highly localized changes in electrical potential during translocation of the negatively charged DNA (Figure 2b). Thus, the ionic- and electronic-conductance responses are highly synchronous during translocation of the DNA. Moreover, the results indicate that the response speed of the nanowire transistor is as fast as that of the nanopore system.

Chemical point decoration is another reliable strategy to build single-molecule FETs. During device fabrication, a

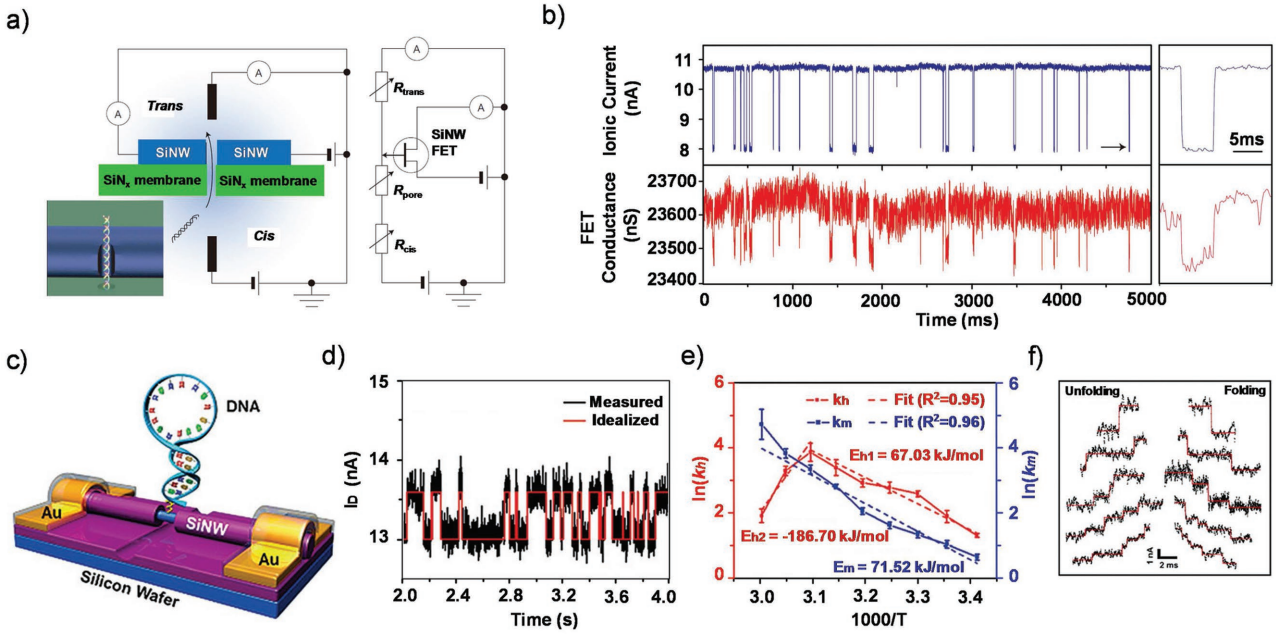

Figure 2. Nanowire-based single-molecule electrical detection. a) Schematic and equivalent circuit diagram of a nanopore–nanowire model. b) Real-time ionic current and FET conductance when double-stranded DNA passes through the nanopore. The right-hand-side panels show an expanded view of blockages indicated by the black arrow. c) Schematic of a nanowire biosensor for folding/unfolding of hairpin DNA. d) Conductance profile of the nanowire device with hairpin DNA. The idealized data are plotted in red. e) Non-Arrhenius and Arrhenius behaviors in the folding/unfolding process. f) Stepwise current changes during unfolding/folding, revealing formation/dissociation of one or several base pairs. a,b) Reproduced with permission.[27] Copyright 2012, Nature Publishing Group. c–f) Reproduced with permission.[28] Copyright 2016, Wiley-VCH.

lithographical gap exposes a micro-region on a CVD-grown silicon nanowire. After annealing the nanowire under an octadecyltrichlorosilane vapor to reduce nonspecific absorption, aminophilic functional groups such as carboxyls,[28] aldehydes,[26] or isothiocyanates[29] are attached to the sidewalls of the nanowire to bind target molecules with amino groups. For example, the folding/unfolding of hairpin DNA with single-base resolution can be monitored in real time.[28] A hairpin-DNA molecule with amino termination at the 5'-end and with five base pairs in the stem and fifteen bases in the loop can be attached to the sidewalls of a silicon nanowire in an aqueous solution at pH = 7.4 (Figure 2c). Two-level conductance fluctuations are then observed (Figure 2d), where the low and high conductances correlate with the hairpin and single-stranded coil states, respectively. The difference in conductance is possibly the result of scattering and/or charge transfer originating from the hairpin DNA. The DNA is the single defect in the nanowire, and transmission at the defect is sensitive to the hairpin conformation. The fraction of the single-stranded coil state increases with temperature, which is in agreement with melting curves of hairpin DNA molecules measured via bulk UV–vis absorption. Non-Arrhenius and Arrhenius-like behaviors are observed for the folding and unfolding processes, respectively (Figure 2e). The non-Arrhenius behavior indicates that the folding is governed by enthalpy at low temperatures and by entropy at high temperatures, which is analogous to protein folding. The randomness parameters of the folding/unfolding duration times were much less than one, indicating that both processes are multi-step processes. Furthermore, the DNA hybridization is captured base-by-base at 20 °C, which is much lower than the melting temperature. Stepwise current fluctuations are occasionally observed with a fine structure of one to five steps (Figure 2f). Each step consists of formation or dissociation of one or several base pairs, thus realizing the folding/unfolding process with single-base resolution.

3.2. Carbon-Nanotube Platforms

Single-walled carbon nanotube (SWNT)-based FET devices have been developed for monitoring the dynamics of single molecules, including chemical interactions and conformation changes. This is because of their ≈1–2 nm diameters, high sensitivity to surrounding charges, and fast response speeds. Specifically, a single target molecule is attached to the SWNT surface via chemical functionalization[30] or physical absorption.[2,31] It can modulate the SWNT conductance through charge scattering or surface-charge-induced gating. Therefore, molecular motions with faint variations in charge distribution can be monitored at the single-molecule level.

Molecules chemically attached to the SWNT modulate the current via charge scattering. Initially, a carboxylate is irreversibly bonded to the SWNT by an electrochemical acid and $KMnO_4$ oxidation. The SWNT conductance markedly decreases because of enhanced scattering at the defect site (**Figure 3**a).[32]

The reaction between the nucleophilic carboxylate and carboxylate-selective molecules such as 1-ethyl-3-(3-dimethylaminopropyl) carbodiimide hydrochloride (EDC) can be monitored by the SWNT device because the reactive EDC-carboxyl intermediate alters the scattering at the defect site. The carboxylate

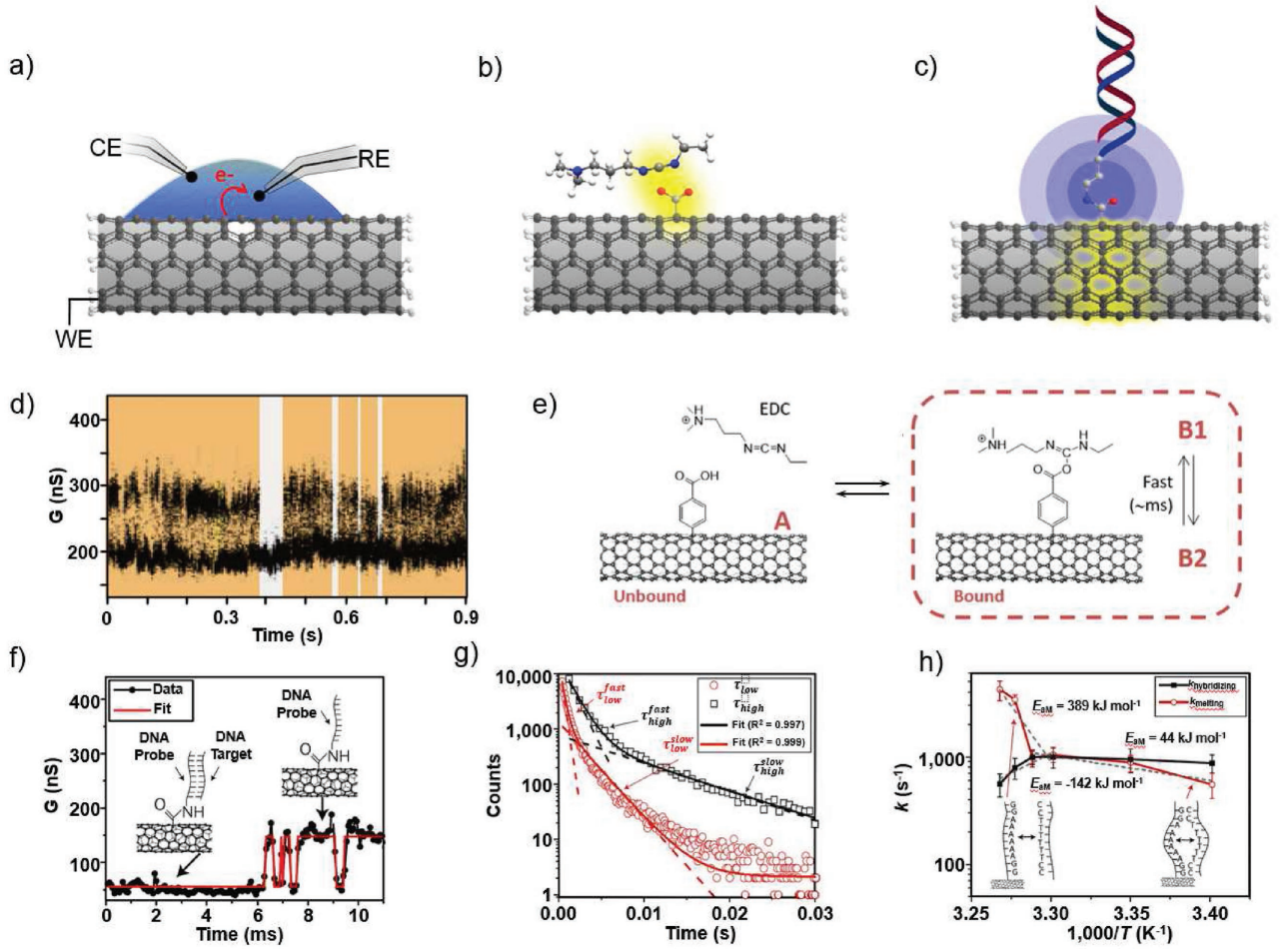

Figure 3. SWNT-based single-molecule electrical devices. a) Schematic of carboxylate functionalization of SWNTs. b) Schematic of carboxyl group on an SWNT for detection of EDC. c) Schematic of DNA attached to an SWNT via chemical functionalization, which can modulate the SWNT conductance via charge scattering. d) Real-time conductance of carboxylic-acid-functionalized SWNT in solution containing 50×10^{-6} M EDC. The orange and gray areas represent active and inactive periods, respectively. e) States of unbound carboxylic probe during inactive periods with conductance A, and active periods (bound) where the conductance fluctuates between two levels B1/B2. f) Real-time conductance of a single-DNA/SWNT device along with idealized data (red), with depictions of the bound and unbound states of the attached DNA probe. g) Double-exponential fits of fast and slow kinetic modes. h) Non-Arrhenius behavior of probe DNA (H_2N-5′-GGAAAAAAGG-3′) because of bubble kinetics at low temperatures. a) Reproduced with permission.[32] Copyright 2007, American Association for the Advancement of Science. b,d) Reproduced with permission.[33] Copyright 2008, American Chemical Society. c,f–h) Reproduced with permission.[30] Copyright 2011, Nature Publishing Group. e) Reproduced with permission.[34] Copyright 2016, American Chemical Society.

is derived from either the SWNT itself[33] (Figure 3b) or a carboxyphenyl probe covalently attached to the nanotube.[34] In both experiments, the real-time conductance trajectory (Figure 3d) can be distinguished by active periods with rapid two-level random noise (orange areas), or inactive periods (gray areas). The alternating active and inactive periods indicate catalyzed EDC hydrolysis; i.e., the active and inactive periods correspond to the presence of the EDC-carboxyl intermediate or the unbound carboxyl (Figure 3e). The rapid two-level fluctuation B1/B2 results from the strong interaction between the SWNT and the acylisourea, which can be regarded as a trap state near the nanotube, analogous to silicon oxide traps. The duration of the active periods is 12.4 s, which is comparable to the 100 s lifetime of EDC in the UV–vis bulk experiment. The fast turnover results from the large excess of EDC and the very low concentration of carboxylate.

The characterized carboxyl/EDC interaction signal is an important signature of carboxylic groups on SWNTs, which could be used for other applications. For example, a single-stranded probe DNA molecule with an amine terminal can be covalently attached to the carboxyl site via amidation (Figure 3c).[30] When a complementary DNA strand is introduced, two-level conductance fluctuations can be observed at temperatures corresponding to DNA hybridization or melting (Figure 3f). Because the charged double-stranded DNA induces enhanced scattering, the high-conductivity and low-conductivity states of the device correspond to unbound and duplex states of the attached DNA, respectively. The temperature-dependent single-DNA hybridization detected with the SWNT device yields enthalpy, entropy, and melting-temperature values that are consistent with ensemble UV–vis measurements. In addition, the device can provide detailed

dynamics of DNA hybridization that are hidden in ensemble measurements. In particular, a memory effect is observed in the hybridization that derives from the competing pathways of three-dimensional diffusion and non-specific adsorption, followed by surface diffusion. Both fast and slow kinetics occur in the conductance signals that can be fitted with double-exponential functions (Figure 3g). Furthermore, other detailed DNA melting processes can be distinguished from the kinetics. For most DNA probes with random sequences, such as H_2N-5′-GTGAGTTGTT-3′, a classical Arrhenius behavior is observed, indicating a direct cracking process. For non-randomly coded DNA probes, such as NH_2-5′-GGAAAAAAGG-3′, a non-Arrhenius behavior occurs because of subtle bubble dynamics during the A–T region at low temperature (Figure 3h). Functionalized SWNT devices have also successfully monitored the folding of a DNA G-quadruplex.[34]

Single-molecule enzyme kinetics has been monitored via charge-induced gating for a biomolecule bound to a SWNT by physical adsorption.[2,31,35,36] Specifically, a genetically engineered enzyme was expressed with a cysteine-group attachment site instead of the wild-type protogenic group. The attachment site was required to have minimal motion during reactions, and one or more charged groups were expected to be present near the attachment site. Then, a single-variant enzyme was attached to the SWNT with an N-(1-pyrenyl)-maleimide linker molecule. The thiol in the cysteine group reacted with the maleimide group of the linker to form a stable thioester bond, and the pyrene group on the other side of the linker was bound to the SWNT through strong π–π stacking. The changing spatial charge distribution of the absorbed enzyme during the reactions can modulate the SWNT conduction via charge-induced gating. Thus, real-time monitoring of molecular motions can be detected by fluctuating SWNT conduction.

An example of the above scenario[2] uses a single T4 lysozyme variant (C54T/C97A/S90C) attached to an SWNT via a linkage molecule (**Figure 4**a,b). The catalytic activity of the attached lysozyme was monitored by the random two-level signal, where low and high conductances corresponded to open and closed lysozyme states, respectively. A slow 15 Hz rate for catalytic turnover and a fast 316 Hz rate for nonproductive enzyme movement were observed (Figure 4c). In addition, by analyzing the randomness of the low states ($r_{low} \approx 1$), it could be deduced that the closing reaction was governed by a simple, single-step Poisson process, whereas the randomness of high states ($r_{high} < 1$) indicates a complex process with at least two opening steps.

To examine the charge-induced SWNT gating mechanism for monitoring single-lysozyme activity, solvent effects and space-charge characteristics of lysozyme variants were systematically studied.[31] In the phosphate buffer (10×10^{-3} M, 50×10^{-3} M NaCl), the SWNT was electrostatically screened by a 1.0 nm Debye layer. Changes in the lysozyme space charge could be detected only in the screening layer. The positively charged K83 and R119 sites in the lysozyme, which were near the C90 attachment site, were expected to electrostatically induce charge gating of the SWNT conductance. During the closing motion of the lysozyme catalysis, both positive residues moved 0.15 nm

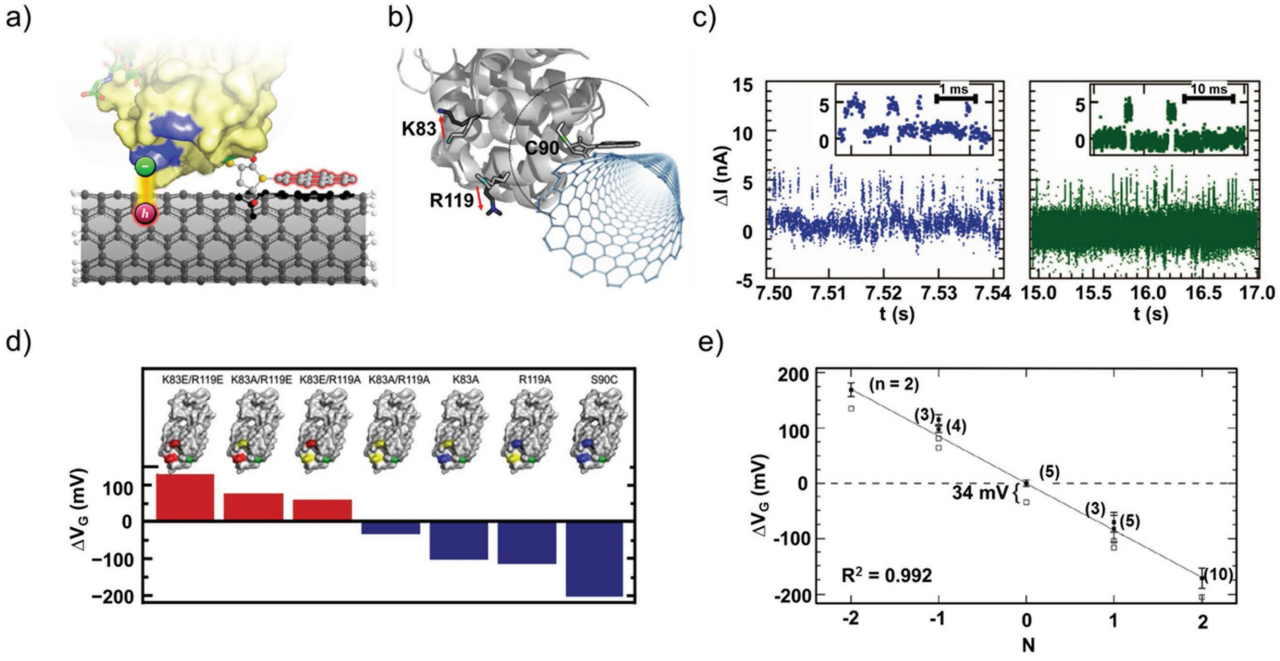

Figure 4. Monitoring the activity of a single lysozyme with an SWNT device. a) Schematic of lysozyme physically adsorbed to an SWNT, which can affect its conductance via charge-induced gating. b) Detailed structure of the lysozyme–SWNT interface. Positively charged K83 and R119 sites, close to the C90 binding site, move substantially during reactions. c) Two-level random signals for the single-lysozyme/SWNT device. The fast mode (left) and the slow mode (right) correspond to catalytic and nonproductive lysozyme motions, respectively. d) The 83 and 119 positions had positive (blue), neutral (yellow), or negative (red) charged side chains, resulting in various values of ΔV_G. e) For all variants, ΔV_G is nearly proportional to the total charge number (N) at positions 83 and 119. a,c) Reproduced with permission.[2] Copyright 2012, American Association for the Advancement of Science. b,d,e) Reproduced with permission.[31] Copyright 2013, American Chemical Society.

away from the SWNT (Figure 4b), which weakened the positive electrostatic field and enhanced the hole current for p-type SWNT.[37,38] When the K83 and R119 sites were replaced by neutral (alanine) or negative (glutamate) chains relative to T4 lysozyme variants (insets of Figure 4d), then reversed gating was obtained for the negative sites and only faint gating was obtained for the neutral sites (K83A/R119A). Furthermore, the effective change in gate voltage (ΔV_G) was linear with the total number of charges in positions 83 and 119 (Figure 4e), which provided strong evidence for charge-induced gating.

In addition to charge-induced gating, charge scattering at the lysozyme attachment point substantially decreased the SWNT conductance. The size of the attachment site was quite small relative to the overall SWNT length. Therefore, the FET signal transduction was not governed by normal gate-induced carrier accumulation. Here, the height and/or width of the scattering barrier affecting SWNT conduction was generated at the attachment site and was modulated by charges on the enzyme.

3.3. Atomically Thin Nanoribbon Platforms

Atomically thin two-dimensional materials, such as graphene and MoS_2, are ultrasensitive for the detection of trace analytes due to their highly active surface area. In particular, atomically thin nanoribbons formed from these materials, as one-dimensional nanotransistors, are predicted to provide single-molecule sensitivity. Although nanoribbons are quite similar to nanotubes in morphology, numerous experimental[39] and theoretical[40–43] results have showed that the conductance of nanoribbons is mostly modulated by surface-charge-induced gating, rather than charge scattering, which is inevitable in SWNT devices. For example, planar molecules such as nucleobases[39,43] or aromatic compounds[43] interact with the surface of nanoribbons via π–π interaction. This interaction may cause a slight alteration to the electronic structure of nanoribbons and thus the conductance. Such a mechanism provides a potential strategy for DNA sequencing, although the selectivity and the operation of real-time monitoring are still challenging. To do this, adopting nanoribbon–nanopore structures may be an effective solution. As shown in **Figure 5**a, single-stranded DNA translocation through the nanopore in a graphene nanoribbon makes it possible to sense nucleobases in the real time.[41] Furthermore, the edges of nanopores are easily functionalized in a chemical way to increase the selectivity (Figure 5b).[44] In addition to the conductance modulation, the interaction between single-stranded DNA molecules and nanoribbons can also realize DNA sequencing, which relies on strain (Figure 5c)[44] or nanomechanical displacement detection (Figure 5d).[45]

4. Electronic Platforms based on Single-Molecule Junctions

Tunneling junctions formed by single molecules have also been widely used for monitoring molecular processes.[46–48] In this

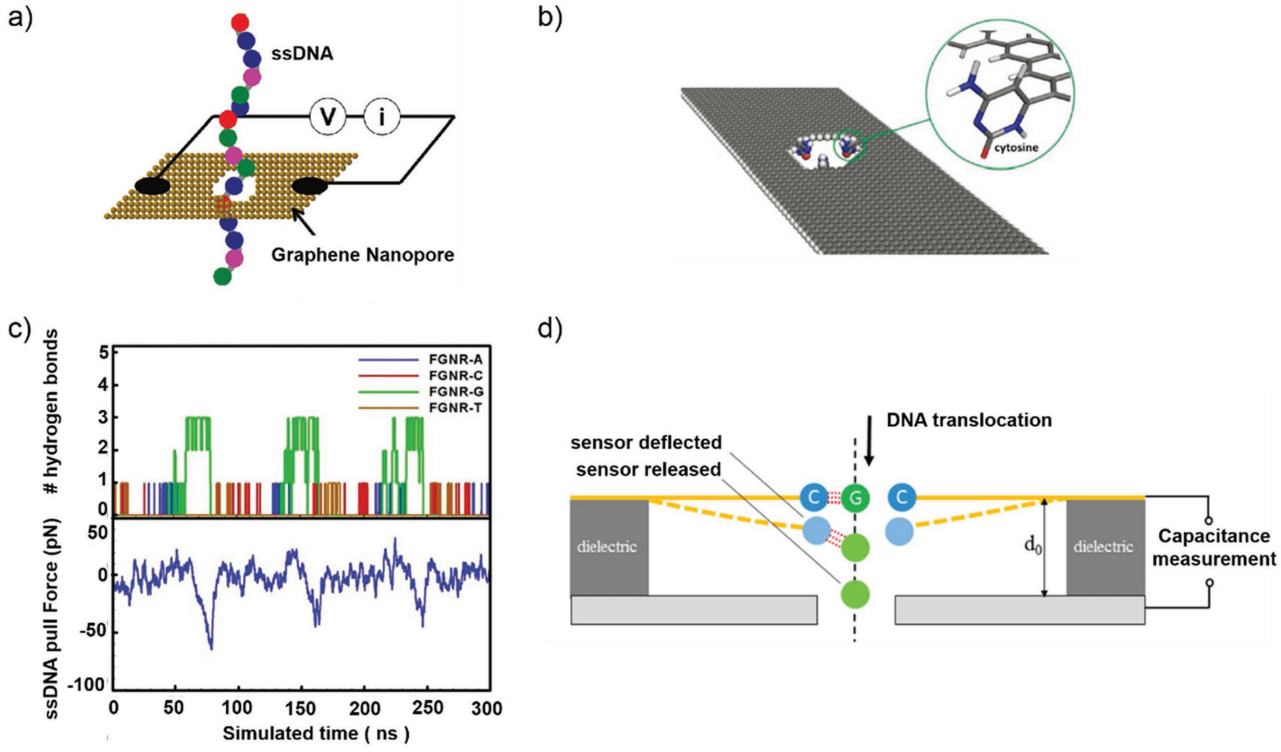

Figure 5. Atomically thin nanoribbons used for single-molecule sensing. a) Schematic of the nanoribbon–nanopore structure. b) Schematic of chemical modification at the edge of the nanopore, where cytosine groups are modified to sense guanine. c,d) DNA sequencing by strain (c) and nanomechanical displacement detection (d). a) Reproduced with permission.[41] Copyright 2010, American Chemical Society. b,c) Reproduced with permission.[44] Copyright 2016, Royal Society of Chemistry. d) Reproduced with permission.[45] Copyright 2016, American Chemical Society.

case, a single-molecule junction (SMJ) is used as a conducting channel and changes in the molecular states are directly transduced into a distinguishable electronic signal.[49–52] Hence, an SMJ can be used for molecular recognition or real-time monitoring of structural transformations. SMJ conductance has more-widespread applications than FET devices, especially for investigating charge-free or small molecules.

4.1. Applications to Single-Molecule Physics

One SMJ approach is to fix target molecules into fabricated nanogaps. Efficient immobilization can lead to continuous monitoring of target dynamics. Structural transformations or interactions with external molecules can thus be detected by variations in conductance through the fixed target molecule. In particular, stable SMJs have been fabricated by using stable amide bonds across SWNT or graphene nanogaps.[53,54]

Host–guest interactions at the single-molecule level between a fixed crown ether in a graphene nanogap and electron-deficient guest molecules in solution have been studied by real-time monitoring[55] (**Figure 6**a). Initially, indented graphene electrodes with gaps of ≈2 nm and carboxy-terminated point contacts were fabricated via dash-line lithography. Then, bis-*p*-phenylene[34]crown-10 (BPP34C10), which contains a crown ether group, was covalently attached to the point contacts with a p-phenylenediamine linkage, thus forming a graphene SMJ. When the SMJ was exposed to a solution containing methyl viologen (MV^{2+}), the formation of a host–guest complex between the MV^{2+} and the crown group on the SMJ significantly

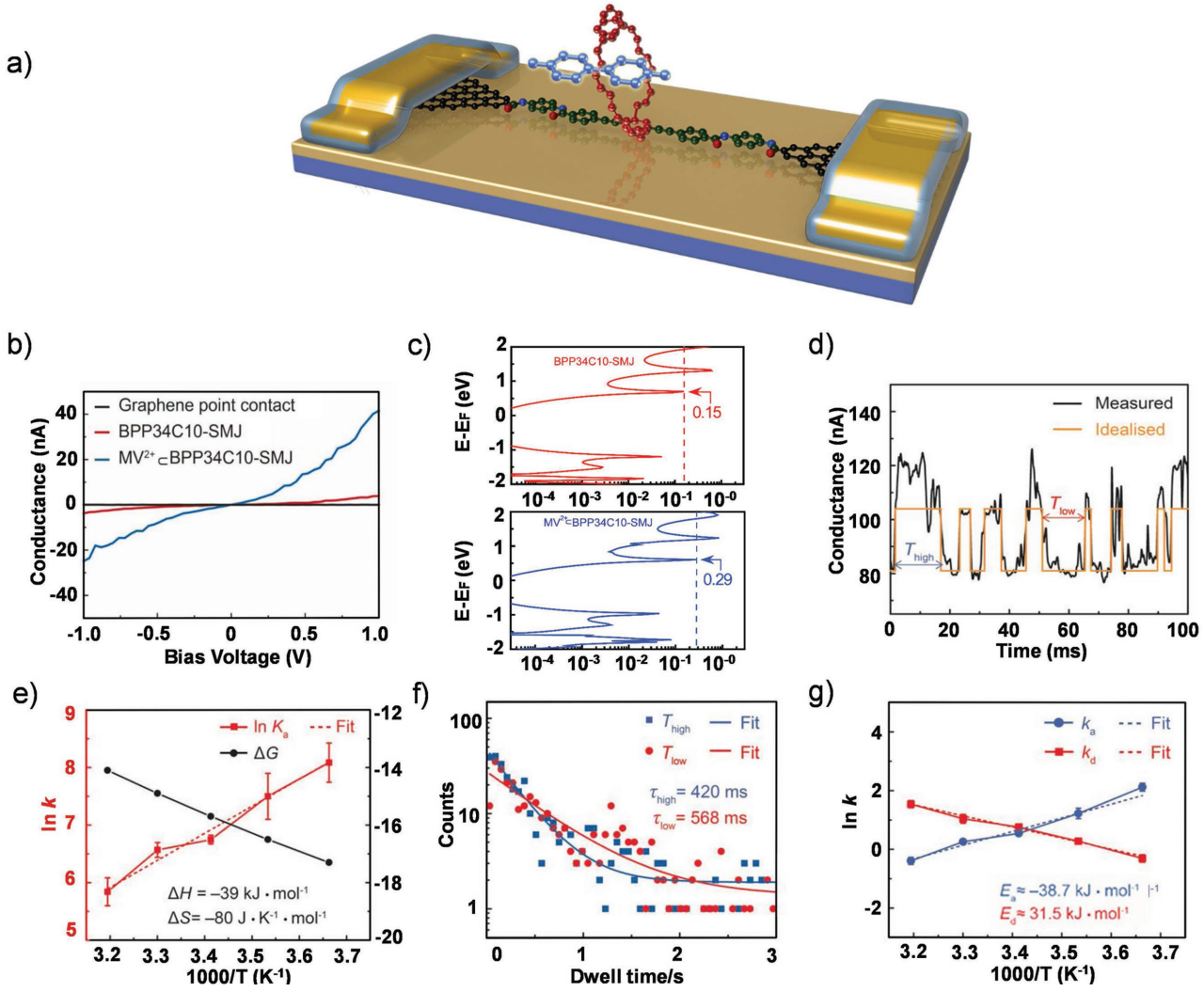

Figure 6. Host–guest interactions via a single-molecule junction. a) Schematic of a graphene–molecule junction, where a single crown ether host molecule is connected to a graphene nanogap for detecting interactions with a methyl viologen guest. b) *I–V* curves for graphene nanogap electrodes (black curve), with BPP34C10-SMJ (red curve), and with MV^{2+}⊂BPP34C10-SMJ (blue curve).(c) Transmission spectra of BPP34C10-SMJ and MV^{2+}⊂BPP34C10-SMJ at zero bias voltage. d) Time–conductance profile for monitoring reversible formation of a MV^{2+}⊂BPP34C10 pseudo-rotaxane complex. e) Plots of ln*K* and Δ*G* vs 1000/*T* deduced from single-molecule measurements. f) Distribution of dwell times for "high" and "low" states. The distribution is a single exponential that yields average dwell times of the two states. g) Arrhenius plots of dissociation and association rate constants that yield activation energies. a–g) Reproduced with permission.[55] Copyright 2016, American Association for the Advancement of Science.

enhanced the SMJ conductance (Figure 6b). In order to understand the variation in molecular conductance, transmission spectra of the two states were calculated by density functional theory (Figure 6c). The larger conductance for the complex is attributed to the lowest unoccupied molecular orbital (LUMO) of the pseudo-rotaxane MV^{2+}⊂BPP34C10 complex, whose spectral peak is nearly 1.93 times larger than that of BPP34C10. Furthermore, detailed pseudo-rotaxane formation and rupture were monitored in real time. As shown in Figure 6d, two-state conductance fluctuations were observed, which corresponded to reversible MV^{2+}⊂BPP34C10 pseudo-rotaxane formation. Thermodynamic and kinetic aspects of these host–guest interactions were characterized by temperature-dependent measurements. From a Gibbs' free-energy analysis at different temperatures (Figure 6e), the change in enthalpy $\Delta H = -39$ kJ mol^{-1} and the change in entropy $\Delta S = -80$ J mol^{-1} K^{-1}. Thus, the association was enthalpy-driven, which was consistent with ensemble-averaged ^{1}H-NMR titrations. The duration times of the events (Figure 6f) revealed that the dwell-time distribution was a single exponential, which indicated first-order kinetics. The kinetic constants for association or dissociation at different temperatures revealed Arrhenius behavior with respective activation energies of $E_a = -38.7$ kJ mol^{-1} and $E_d = 31.5$ kJ mol^{-1} (Figure 6g).

Electron-transfer dynamics in an SMJ can also be monitored in real time. For example, an SMJ with a diarylethene core was attached to graphene[56] (**Figure 7**a) with a weak coupling such that the diarylethene core had no interference from the electrodes aside from the photoinduced switching due to the electrocyclic reactions of the diarylethene molecule (Figure 7a). Stochastic switching was observed over the temperature range 160–240 K in the closed state of the diarylethene (Figure 7b). The bistable fluctuations were attributed to electron-transfer processes where the low state represented the neutral molecule and the high state represented the cationic molecule formed by transient molecular charge transfer from the highest occupied molecular orbital (HOMO). The latter changed the diarylethene conformation, which resulted in significant differences in conductance. The dynamics of electron transfer were investigated at different bias voltages. The duration of the high state increased with bias voltage, while the duration time of low state decreased; this means that the high-polarity cationic molecule formed more easily and was more stable in a strong electrostatic field (Figure 7c). The electron-transfer dynamics were also investigated as a function of temperature. The occurrence ratio of the high state increased with temperature, illustrating that the free energy of the electron transfer was determined by entropy. Specifically, the changes in enthalpy and entropy were $\Delta H = -0.37$ eV and $\Delta S = 1.9$ meV K^{-1} (Figure 7d). The electron-transfer dynamics were determined by k_BT and the barrier height ΔE. At temperatures lower than 160 K, $k_BT << \Delta E$; thus, one state dominates and electron transfer barely occurs. At 160–240 K, k_BT was comparable to ΔE and electron transfer occurred. The kinetic constant of charging/discharging increased with the temperature (Figure 7e). At temperatures higher than 240 K, $k_BT >> \Delta E$: electron transfer was thermodynamically controlled and the switch again disappeared.

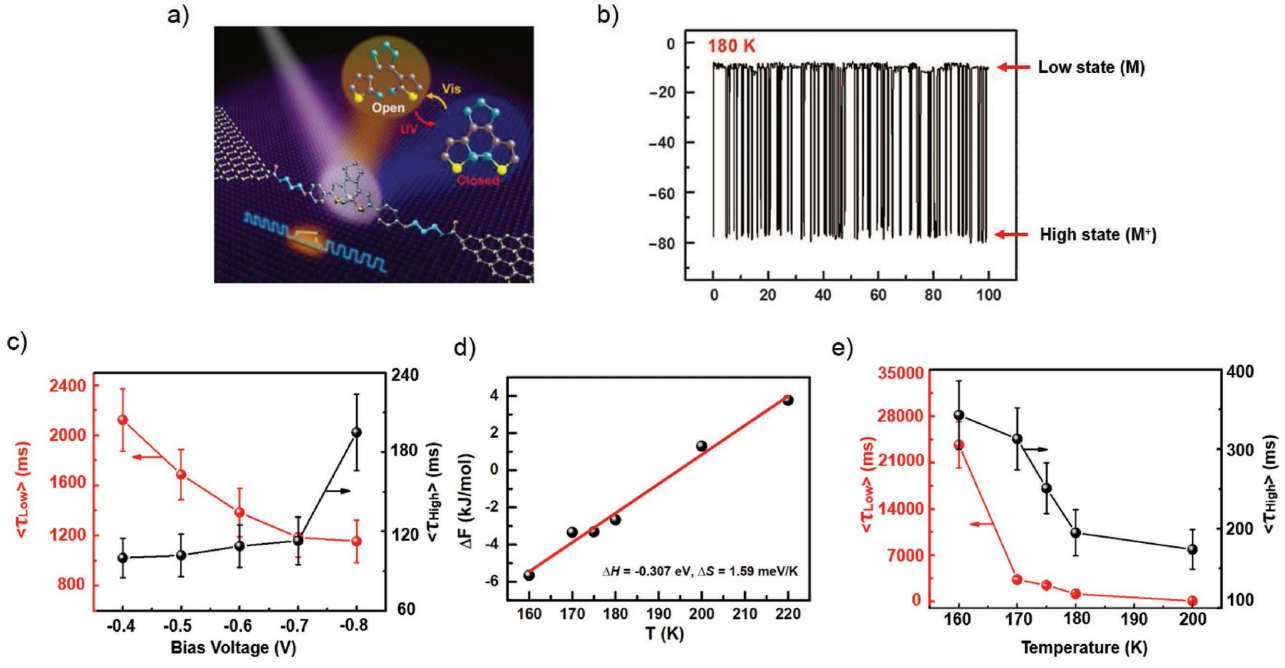

Figure 7. Single-molecule junction for investigating electron-transfer dynamics. a) Schematic of an SMJ where a diarylethene molecule is connected to a graphene nanogap. The diarylethene core changes between an open form and a closed form via photoinduced electrocyclic reactions. b) Stochastic switching at 180 K when the diarylethene core is in its closed form. The low and high states represent neutral (M) and cationic (M^+) forms. c) Mean durations of the low and high states at different bias voltages. d) Thermodynamic analysis of temperature-dependent electron transfer. e) Mean durations of the low and high states vs temperature. a,b) Reproduced with permission.[56] Copyright 2016, American Association for the Advancement of Science. c–e) Plotted from data in ref. [56].

4.2. Applications to Single-Molecule Recognition

Another example of SMJ applications is the detection of target molecules flowing through the nanogap. This has been widely implemented to detect amino acids,[57] single peptides,[6,57] nucleotides,[58–60] DNA oligomers,[61] and DNA chains.[62,63] When the target molecules in solution flow through the nanogap of tunneling electrodes, the density-of-states (DOS) overlap between the electrodes and the trapped molecule will lead to electrical signals for single-molecule detection. Because the tunneling current is determined by the intrinsic characteristics of the passing target, it is a fingerprint for molecular recognition. The first important parameter is the junction conductance, which depends on the electronic structure of the trapped molecule as well as the matched DOS between the molecule and the nanogap electrodes. Another important parameter is the duration time of the current pulse, which mainly depends on the interaction between the molecule and the electrodes.

Reliable molecular recognition with a tunneling junction requires a molecular-scale gap between the electrodes. Fabrication techniques for making these nanogap electrodes have been based on scanning tunneling microscopy (STM),[59,61] electromigration,[64] mechanically controllable break junctions (MCBJs),[6] carbon nanowires,[65] or multilayer structures.[58] With a precisely controlled gap to fit the target molecule, single-molecule detection can be realized with a tunneling junction.

Taniguchi et al. used MCBJs to study nucleotides (**Figure 8**a).[60,66] When a target DNA or RNA base diffused through the 0.8 nm MCBJ gap, a current pulse was detected. Because of their different HOMO energies, four different DNA or RNA bases could be distinguished by the current pulses (Figures 8c,d). The tunneling junctions were able to precisely discriminate nucleotides from oligomers in DNA trimers. Furthermore, when a microRNA 5′-UGAGGUA-3′ passed through the nanogap, its full sequence characteristic was obtained (Figure 8e). Thus, tunneling junctions have the potential to be used for nucleotide sequencing.

MCBJ tunneling junctions have also been used for amino-acid recognition (Figure 8b),[6] which is more complex because of the broad variety of structures. Fabricated 0.7 nm and 0.55 nm gaps were used for detecting the twenty amino acids.

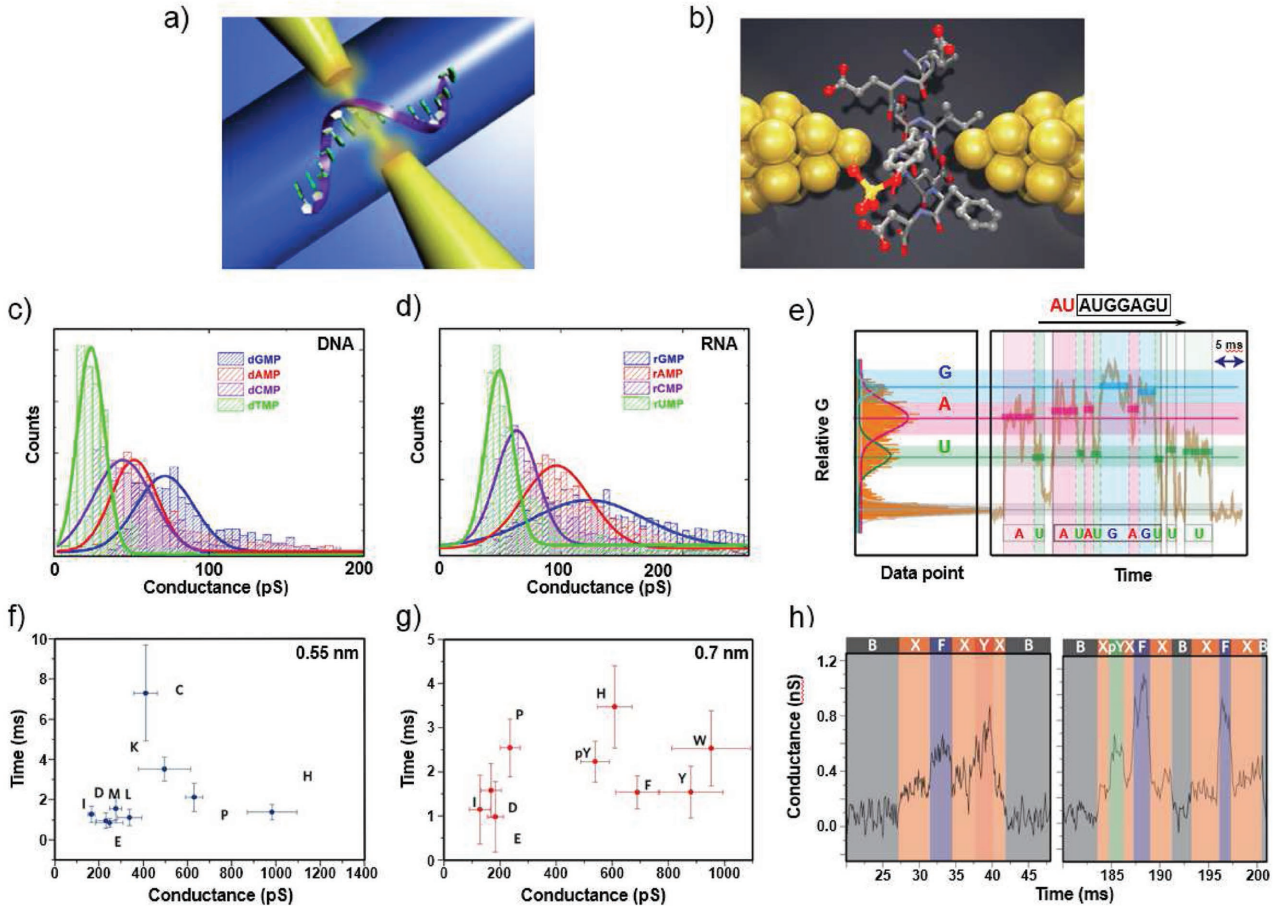

Figure 8. Molecular recognition in MCBJ-based tunneling junctions. a,b) Schematic of MCBJ junctions for detecting trapped nucleic acids (a) or amino acids (b) in the nanogap. c,d) Characteristic conductance histograms for four DNA deoxynucleoside monophosphates (c) and four nucleoside monophosphates of RNA (d). e) Relative conductance (G) histograms and corresponding G–t profiles for re-sequencing of 3′-AUGGAGU-5′ microRNA. f,g) Two-dimensional plots of conductance and duration time, measured with 0.55 nm (f) and 0.7 nm (g) gap electrodes, are analyzed as fingerprints for thirteen amino acids. h) Typical conductance–time profiles for IEEEIYCEFD and IEEEIpYCEFD peptides. a,c–e) Reproduced with permission.[66] Copyright 2012, Nature Publishing Group. b,f–g) Reproduced with permission.[6] Copyright 2014, Nature Publishing Group.

Except for the DOS overlap between the target molecule and the electrodes, nanogap size fitting had a great effect on molecular recognition. Specifically, the 0.7 nm gap was sensitive to large amino acids, while the 0.5 nm gap was sensitive to small ones. From the molecular conductances and duration times (Figures 8f,g), where the amino acids and their distinctive tunneling behaviors are intuitively associated, more than seven amino acids could be recognized from their tunneling signals. From this capability, both the amino-acid types and their mixing ratios in solution could be identified from specific tunneling signals. Furthermore, peptide sequences could also be partially confirmed. For example, when a peptide with the sequence IEEEIYCEFD passed through the nanogap, a specific conductance–time profile was observed (Figures 8h). Conductance terraces at 722 ps and 566 ps corresponded to Y (tyrosine) and F (phenylalanine), respectively; and that at 222 ps to nondifferentiable C (cysteine), I (isoleucine), E (glutamic acid), D (aspartic acid), which are labeled X. Thus, the peptide was re-sequenced as XYXFX, which conformed to the peptide sequence. The peptide sequencing ability of tunneling junctions was again confirmed with the sequence IEEEIpYCEFD, where F and pY (phosphorylated tyrosine) amino-acid units were recognized from the peptide (Figure 8h). In addition, the IEEEIYCEFD and IEEEIpYCEFD peptides in mixed solution could be distinguished with tunneling signals, which demonstrated that the tunneling can detect tyrosine phosphorylated variants in peptides.

In order to improve tunneling junctions, Lindsay et al. combined STM with specific molecular recognition for single-molecule detection (**Figure 9**a).[57,61] Specifically, gold tips and substrates were chemically modified with 4-mercaptobenzamide, which had a thiol group attached to a gold electrode and an amide group for molecular recognition. Through hydrogen-bond interactions, target molecules such as DNA oligomers or amino acids, could be trapped in tip–substrate nanogaps, which led to tunneling current spikes. The intrinsic energy levels and DOS differences of A, T, C, G nucleotides in DNA nucleotides passing through the nanogap created different matching modes for the four nucleotides that (Figure 9b) led to specific pulse currents with different distributions and total count rates. The pulse currents were highly correlated to specific nucleotides. Thus, the technique was able to identify single bases in a DNA oligomer, including methylation variants. The same parameters of current distribution, duration times, or total count rates could not provide enough resolution to distinguish amino acids. A machine-learning algorithm was utilized to pick out specific amino acids from the tunneling signals. Single-component samples of all the amino acids were used to train the algorithm. It was then able to recognize specific amino acids in mixtures, including chiral enantiomers, isobaric isomers, and methylated variants. For example, Fourier amplitude distributions for pure D- and L-asparagine (Asn) over the interval of 19–22 kHz (Figure 9c) were used to train the algorithm. Thus, D- and L-Asn were distinguished from the mixture of tunneling current spikes (Figure 9d). In addition, the asparagine L/D ratio was quantitatively analyzed (Figure 9e).

Single-molecule recognition via tunneling has potential applications for detecting molecules with complex secondary structures, such as short-chain DNA or peptides, which would complement sequencing. However, it has shortcomings such as the stochastic Brownian diffusion of molecular chains through the tunneling nanogap, which causes random fragment sequences. Furthermore, the chains may move back and forth through the nanogap, which duplicates detection. Nanopores

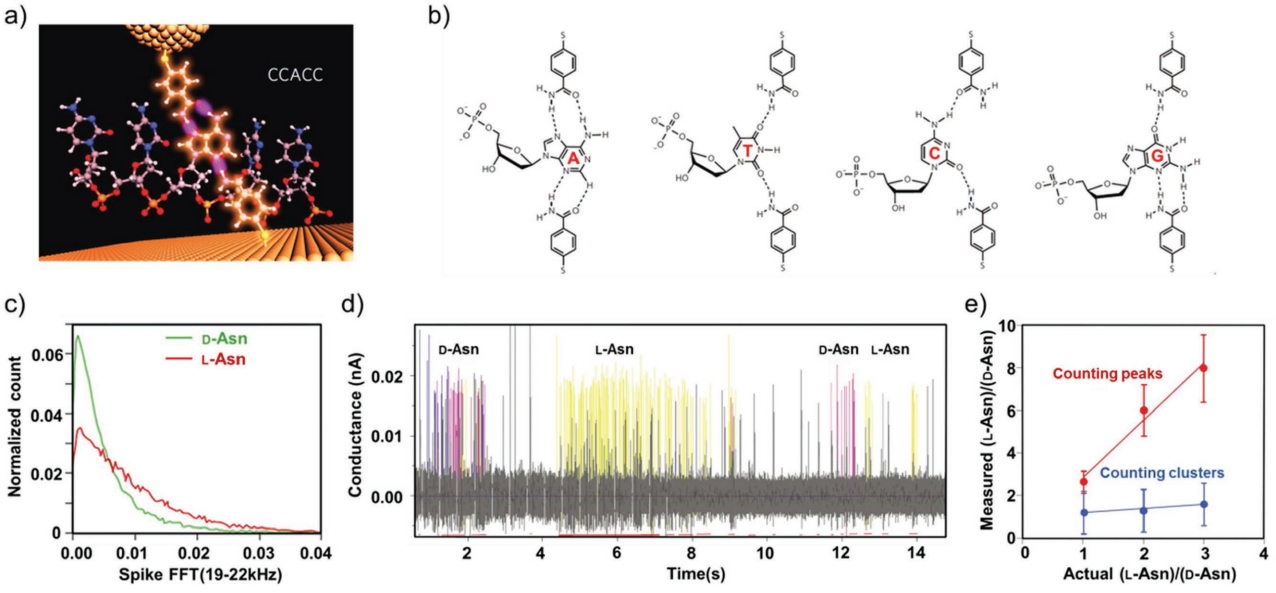

Figure 9. STM-based molecular recognition. a) Schematic of an STM tunneling junction with specific recognition molecules on a gold tip and a substrate for detecting DNA oligomers via hydrogen-bond interactions. b) Schematic for matching modes between the four nucleotides and the recognition molecule. c) Fourier amplitude distributions for D-Asn and L-Asn tunneling current spikes over 19–22 kHz. d) Tunneling signals for a 1:1 mixture of D-Asn and L-Asn. Assignments are coded in purple (D-Asn) and yellow (L-Asn), and black spikes are unassigned. e) Quantification of the D/L ratio using an algorithm trained with pure samples, where the measured ratio is consistent with the actual ratio. a,b) Reproduced with permission.[61] Copyright 2010, Nature Publishing Group. c–e) Reproduced with permission.[57] Copyright 2014, Nature Publishing Group.

can constrain single molecular chains to pass through unidirectionally, as practiced in FET nanowire–nanopore structures.[27,65] Thus, introducing a nanopore to the tunneling junction may be necessary to control molecular chain diffusion through the nanogap.

4.3. Applications to Electrostatic Catalysis

Recent theoretical studies suggested that electrostatic fields can affect chemical reactions, especially pericyclic reactions. It is very hard to verify in bulk because the field intensity is limited and molecular orientations are uncontrollable. However, SMJs are suitable platforms to investigate electrostatic catalysis because the molecules are controllably orientated on the electrodes and the electrode gap provides a strong electrostatic field of $\approx 10^8$–10^9 V m^{-1}.

STM has been used as a real-time monitor and an in situ controller of single-molecule Diels–Alder reactions. As shown in **Figure 10**a, a conjugated furan diene and dienophile (a norbornylogous bridge) were covalently attached to an STM tip and a flat gold surface, respectively.[67] Because an oriented electric field can easily be realized by STM, electrostatic catalysis of the Diels–Alder reaction can also be controlled by the junction bias. Specifically, when one Diels–Alder reaction occurred between the tip and substrate (insets of Figure 10b), a current jump (blink) was observed (Figure 10b). Furthermore, the statistical relationship between the blinking frequency and the applied bias (Figure 10c) indicated that negative biases significantly accelerated the reaction. Thus, the electric field lowered the reaction barrier. In particular, the transition state of the Diels–Alder reaction has three resonance structures (Figure 10d), where charge separation depends on the relative electronegativities of the reacted diene and dienophile. Therefore, for the "downward" electric-field orientation at a negative bias, resonance structure I was the most likely to be stabilized because the diene was electron-rich and the dienophile was electron-deficient. This conformation had the lowest reaction barrier, and electrostatic catalysis of the Diels–Alder reaction proceeded. Calculations confirmed that this specific transition state had the highest electric-field sensitivity (Figure 10e).

5. Single-Molecule Statistics

Abundant molecular-dynamics information can be obtained through real-time monitoring of the molecular states at the single-molecule level. Therefore, it is of crucial importance to find a universal framework to decode fluctuating electronic signals into fundamental quantities that correspond to macroscopic properties. Because concentration is meaningless for single-molecule processes, dynamic or thermodynamic quantities are not appropriate. However, in most cases, time averaging is equivalent to ensemble averaging. Thus, fundamental quantities can be redefined from the time domain.

Under normal conditions, an elementary single-molecule reaction follows a single-step Poisson process that is stochastic, memory-free, and independent. The duration time between

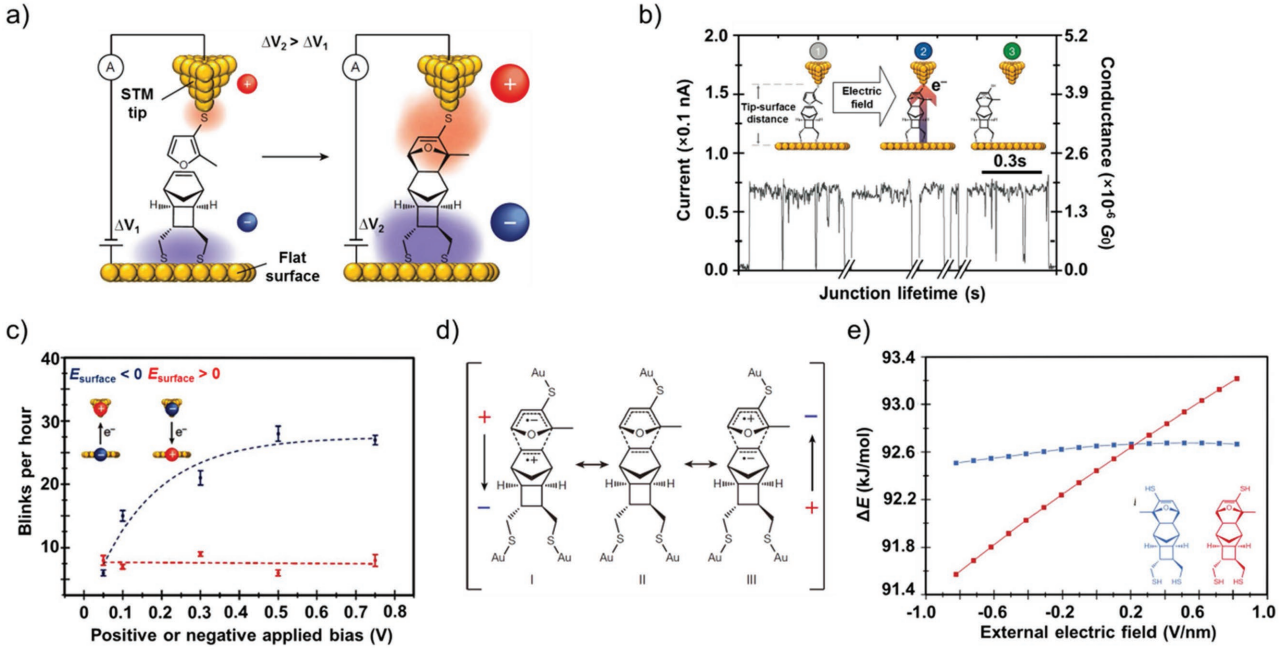

Figure 10. Performing a Diels–Alder reaction with STM. a) Schematic of Diels–Alder reaction under the external electric field of the tip–surface junction. The diene and dienophile are attached to the STM tip and the flat gold surface, respectively, via thiol groups. b) A conductance–time profile for monitoring "blinking" (current pulses) representing single-molecule reactions. The inset shows the stages encountered during a blinking event. c) Frequency of blinking as a function of applied bias. Positive and negative biases are respectively plotted in red and blue. d) Three possible resonance structures of the transition state, where charge-separated structures I or III are more likely to be stabilized by appropriate electric fields. e) Changes in height of the reaction barrier with external electric field. Two kinetically favored products are shown (inset shown in red and blue), where the red one has a strong field sensitivity. a–e) Reproduced with permission.[67] Copyright 2016, Nature Publishing Group.

two turnovers can be extracted and analyzed from a real-time conductance profile (Figure 6d) with the aid of software, such as QuB.[68] The distribution of duration times of events can be fitted with a single exponential:

$$P(\tau) = \frac{1}{\langle \tau \rangle} \exp\left(-\frac{\tau}{\langle \tau \rangle}\right) \quad (1)$$

which defines the mean duration time $<\tau>$. Other fundamental quantities can be calculated from $<\tau>$. For example, the activation energy can be derived via the Arrhenius equation:

$$k_T = k_\infty \exp\left(\frac{-E_a}{RT}\right) \quad (2)$$

where the kinetic constant k_T is the reciprocal of $<\tau>$ at temperature T. The energy difference ΔE between two translatable states can be derived from Boltzmann statistics:[2,33]

$$\Delta E = -RT \ln \frac{\langle \tau_1 \rangle}{\langle \tau_2 \rangle} \quad (3)$$

The Gibbs' free energy (ΔG) can be derived by:

$$\Delta G = -RT \ln K \quad (4)$$

where K represents the equilibrium constant, which must be redefined at the single-molecule level. In first-order reactions, such as enzyme catalysis, ΔG is equivalent to ΔE, with $K = k_1/k_2$. For second-order reactions, such as intermolecular interactions, an extra correction is required concerning the dispersed reactant concentrations. According to the Langmuir isotherm model, which is commonly adopted for immobilized single molecules, the equivalent constant can be written as:

$$K = \frac{\alpha}{1-\alpha} C \quad (5)$$

where α is the fraction of one stable state of the immobilized molecule and C represents the concentration of other interacting molecules dispersed in solution.[30,69] ΔH and ΔS for the two translatable states of the reaction can also be calculated from:

$$\Delta G = \Delta H - T\Delta S \quad (6)$$

which is the same as that for the macroscopic system. According to transition-state theory, ΔH_1 and ΔS_1 for one primary state crossing the transition state can be derived by the van't Hoff equation:

$$R \ln \frac{h}{\langle \tau_1 \rangle k_B T} = -\frac{\Delta H_1}{T} + \Delta S_1 \quad (7)$$

Information hidden in ensemble averages can be derived from a series of single-events. For example, the randomness statistical indicator is widely used to reveal hidden intermediate steps of reactions.[2,28,70] Randomness r is defined as a normalized variance:

$$r = \frac{\sigma^2}{\langle t \rangle^2} = \frac{\sum_i (\tau_i - \langle \tau \rangle)^2}{\sum_i \tau_i^2} \quad (8)$$

where $r = 1$ in a single-step Poisson process, and is $1/n$ in an identical n-step Poisson process.[71]

Covariance parameters of events are other statistical indicators used to determine whether memory effects exist.[72,73] The covariance parameters $r(m)$ are the normalized autocorrelation values of event duration times used to evaluate the correlation of events between $m-1$ turnovers. The covariance parameter can be calculated from:

$$r(m) = \frac{n\sum_i^n \tau_i \tau_{i+m} - \left(\sum_i^n \tau_i\right)^2}{n\sum_i^n \tau_i^2 - \left(\sum_i^n \tau_i\right)^2} = \frac{\langle \Delta t(0) \Delta t(m) \rangle}{\langle \Delta t^2 \rangle} \quad (9)$$

For a stochastic and memory-free Poisson process, $r(0) = 1$; $r(m) = 0$ for $m > 0$; and $r(m) > 0$ when $m > 0$ indicates a positive correlation between adjacent events, i.e., a memory effect. The origins of memory effects include an alterable catalysis activity,[74] an alterable reaction path[30] or mode,[2] a solution effect, or dynamic disorder in an enzyme.[73]

6. Conclusion and Perspective

Here, we have summarized recent significant advances in real-time electrical detection of single-molecule dynamic processes, with a particular focus on one-dimensional nanotransistors and molecular-tunneling junctions, which can transduce single-molecule states into detectable electrical signals. With these platforms, molecular structural characteristics can be recognized. Single-molecule motion and reactions can also be monitored to detect intermediates/transient states and confirm chemical or biological reaction sequences. Statistical analysis of single-molecule signals can be used to determine dynamical parameters that correlate with those for ensemble-averaged reactions. Therefore, intrinsic mechanisms of molecular motion and reactions can be revealed by single-molecule electrical measurements.

Despite the above-mentioned remarkable progress, single-molecule electrical techniques are still in the early stages of the development and have many challenges that need to be overcome. For example, device sensitivity and selectivity need to be enhanced to distinguish detected signals from both background noises and interfering molecules. Chemical functionalization is a promising strategy used to select analytes with specific functional groups. The combination of electrical methods and optical approaches, such as fluorescence or electroluminescence, could be considered to provide another efficient route. This combination might also improve molecule detection in a quantitative way and increase the possibility of device fabrication. Device uniformity should be controlled to reduce discrepancies among different devices, such as SWNT conduction in FET-based devices and nanogap structures in

tunneling junctions. Device-fabrication yields and integration levels should be improved for high-throughput multiplexed detection. The solutions to these challenges may rely on further improvement of robust nanofabrication methodologies in the future, including easy materials synthesis and precise lithographic techniques. With all these improvements, single-molecule electronic-detection techniques will continue to have broad applications in molecular recognition, DNA and protein sequencing, molecule diagnostics, and dynamic monitoring of both chemical and biological reactions, which will invite future intense research activities.

Acknowledgements

C.G. and C.J. authors contributed equally to this work. The authors acknowledge primary financial support from NSFC (21225311, 91333102 and 21373014).

Keywords

molecular recognition, real-time monitoring, single-molecule dynamics, tunneling junctions

Received: January 11, 2017
Revised: February 25, 2017
Published online: April 12, 2017

[1] R. Coontz, B. Hanson, *Science* **2004**, *305*, 957.
[2] Y. Choi, I. S. Moody, P. C. Sims, S. R. Hunt, B. L. Corso, I. Perez, G. A. Weiss, P. G. Collins, *Science* **2012**, *335*, 319.
[3] S. Y. Berezhna, J. P. Gill, R. Lamichhane, D. P. Millar, *J. Am. Chem. Soc.* **2012**, *134*, 11261.
[4] S. Liu, X. Y. Zhang, W. X. Luo, Z. X. Wang, X. F. Guo, M. L. Steigerwald, X. H. Fang, *Angew. Chem., Int. Ed.* **2011**, *50*, 2496.
[5] C. A. Aguilar, H. G. Craighead, *Nat. Nanotechnol.* **2013**, *8*, 709.
[6] T. Ohshiro, M. Tsutsui, K. Yokota, M. Furuhashi, M. Taniguchi, T. Kawai, *Nat. Nanotechnol.* **2014**, *9*, 835.
[7] G. Bonnet, O. Krichevsky, A. Libchaber, *Proc. Natl. Acad. Sci. USA* **1998**, *95*, 8602.
[8] S. T. Hess, S. H. Huang, A. A. Heikal, W. W. Webb, *Biochemistry* **2002**, *41*, 697.
[9] R. Roy, S. Hohng, T. Ha, *Nat. Methods* **2008**, *5*, 507.
[10] J. Eid, A. Fehr, J. Gray, K. Luong, J. Lyle, G. Otto, P. Peluso, D. Rank, P. Baybayan, B. Bettman, A. Bibillo, K. Bjornson, B. Chaudhuri, F. Christians, R. Cicero, S. Clark, R. Dalal, A. Dewinter, J. Dixon, M. Foquet, A. Gaertner, P. Hardenbol, C. Heiner, K. Hester, D. Holden, G. Kearns, X. X. Kong, R. Kuse, Y. Lacroix, S. Lin, P. Lundquist, C. C. Ma, P. Marks, M. Maxham, D. Murphy, I. Park, T. Pham, M. Phillips, J. Roy, R. Sebra, G. Shen, J. Sorenson, A. Tomaney, K. Travers, M. Trulson, J. Vieceli, J. Wegener, D. Wu, A. Yang, D. Zaccarin, P. Zhao, F. Zhong, J. Korlach, S. Turner, *Science* **2009**, *323*, 133.
[11] X. W. Zhuang, H. Kim, M. J. B. Pereira, H. P. Babcock, N. G. Walter, S. Chu, *Science* **2002**, *296*, 1473.
[12] R. D. Vale, *Cell* **2008**, *135*, 779.
[13] Y. D. Yin, X. S. Zhao, *Acc. Chem. Res.* **2011**, *44*, 1172.
[14] J. J. Kasianowicz, E. Brandin, D. Branton, D. W. Deamer, *Proc. Natl. Acad. Sci. USA* **1996**, *93*, 13770.
[15] L. Song, M. R. Hobaugh, C. Shustak, S. Cheley, H. Bayley, J. E. Gouaux, *Science* **1997**, *274*, 1859.
[16] A. J. Storm, J. H. Chen, X. S. Ling, H. W. Zandbergen, C. Dekker, *Nat. Mater.* **2003**, *2*, 537.
[17] A. R. Hall, A. Scott, D. Rotem, K. K. Mehta, H. Bayley, C. Dekker, *Nat. Nanotechnol.* **2010**, *5*, 874.
[18] G. F. Schneider, S. W. Kowalczyk, V. E. Calado, G. Pandraud, H. W. Zandbergen, L. M. K. Vandersypen, C. Dekker, *Nano Lett.* **2010**, *10*, 3163.
[19] H. Bayley, P. S. Cremer, *Nature* **2001**, *413*, 226.
[20] J. Clarke, H.-C. Wu, L. Jayasinghe, A. Patel, S. Reid, H. Bayley, *Nat. Nanotechnol.* **2009**, *4*, 265.
[21] D. Stoddart, A. J. Heron, E. Mikhailova, G. Maglia, H. Bayley, *Proc. Natl. Acad. Sci. USA* **2009**, *106*, 7702.
[22] C. Dekker, *Nat. Nanotechnol.* **2007**, *2*, 209.
[23] D. Branton, D. W. Deamer, A. Marziali, H. Bayley, S. A. Benner, T. Butler, M. Di Ventra, S. Garaj, A. Hibbs, X. Huang, S. B. Jovanovich, P. S. Krstic, S. Lindsay, X. S. Ling, C. H. Mastrangelo, A. Meller, J. S. Oliver, Y. V. Pershin, J. M. Ramsey, R. Riehn, G. V. Soni, V. Tabard-Cossa, M. Wanunu, M. Wiggin, J. A. Schloss, *Nat. Biotechnol.* **2008**, *26*, 1146.
[24] D. Dulin, J. Lipfert, M. C. Moolman, N. H. Dekker, *Nat. Rev. Genet.* **2013**, *14*, 9.
[25] F.-R. F. Fan, A. J. Bard, *Science* **1995**, *267*, 871.
[26] J. D. Wang, F. X. Shen, Z. X. Wang, G. He, J. W. Qin, N. Y. Cheng, M. S. Yao, L. D. Li, X. F. Guo, *Angew. Chem., Int. Ed.* **2014**, *53*, 5038.
[27] P. Xie, Q. Xiong, Y. Fang, Q. Qing, C. M. Lieber, *Nat. Nanotechnol.* **2012**, *7*, 119.
[28] G. He, J. Li, H. N. Ci, C. M. Qi, X. F. Guo, *Angew. Chem., Int. Ed.* **2016**, *55*, 9036.
[29] J. Li, G. He, H. Ueno, C. C. Jia, H. Noji, C. M. Qi, X. F. Guo, *Nanoscale* **2016**, *8*, 16172.
[30] S. Sorgenfrei, C.-y. Chiu, R. L. Gonzalez Jr., Y.-J. Yu, P. Kim, C. Nuckolls, K. L. Shepard, *Nat. Nanotechnol.* **2011**, *6*, 125.
[31] Y. Choi, T. J. Olsen, P. C. Sims, I. S. Moody, B. L. Corso, M. N. Dang, G. A. Weiss, P. G. Collins, *Nano Lett.* **2013**, *13*, 625.
[32] B. R. Goldsmith, J. G. Coroneus, V. R. Khalap, A. A. Kane, G. A. Weiss, P. G. Collins, *Science* **2007**, *315*, 77.
[33] B. R. Goldsmith, J. G. Coroneus, A. A. Kane, G. A. Weiss, P. G. Collins, *Nano Lett.* **2008**, *8*, 189.
[34] D. Bouilly, J. Hon, N. S. Daly, S. Trocchia, S. Vernick, J. Yu, S. Warren, Y. Wu, R. L. Gonzalez Jr., K. L. Shepard, C. Nuckolls, *Nano Lett.* **2016**, *16*, 4679.
[35] K. M. Pugliese, O. T. Gul, Y. Choi, T. J. Olsen, P. C. Sims, P. G. Collins, G. A. Weiss, *J. Am. Chem. Soc.* **2015**, *137*, 9587.
[36] P. C. Sims, I. S. Moody, Y. Choi, C. Dong, M. Iftikhar, B. L. Corso, Q. T. Gul, P. G. Collins, G. A. Weiss, *J. Am. Chem. Soc.* **2013**, *135*, 7861.
[37] S. Liu, J. M. Li, Q. Shen, Y. Cao, X. F. Guo, G. M. Zhang, C. Q. Feng, J. Zhang, Z. F. Liu, M. L. Steigerwald, D. S. Xu, C. Nuckolls, *Angew. Chem., Int. Ed.* **2009**, *48*, 4759.
[38] C. C. Jia, H. Li, J. L. Jiang, J. D. Wang, H. L. Chen, D. Cao, J. F. Stoddart, X. F. Guo, *Adv. Mater.* **2013**, *25*, 6752.
[39] N. Dontschuk, A. Stacey, A. Tadich, K. J. Rietwyk, A. Schenk, M. T. Edmonds, O. Shimoni, C. I. Pakes, S. Prawer, J. Cervenka, *Nat. Commun.* **2015**, *6*, 6563.
[40] S. K. Min, W. Y. Kim, Y. Cho, K. S. Kim, *Nat. Nanotechol.* **2011**, *6*, 162.
[41] T. Nelson, B. Zhang, O. V. Prezhdo, *Nano Lett.* **2010**, *10*, 3237.
[42] H. W. Postma, *Nano Lett.* **2010**, *10*, 420.
[43] A. C. Rajan, M. R. Rezapour, J. Yun, Y. Cho, W. J. Cho, S. K. Min, G. Lee, K. S. Kim, *ACS Nano* **2014**, *8*, 1827.
[44] E. Paulechka, T. A. Wassenaar, K. Kroenlein, A. Kazakov, A. Smolyanitsky, *Nanoscale* **2016**, *8*, 1861.
[45] A. Smolyanitsky, B. I. Yakobson, T. A. Wassenaar, E. Paulechka, K. Kroenlein, *ACS Nano* **2016**, *10*, 9009.
[46] C. C. Jia, X. F. Guo, *Chem. Soc. Rev.* **2013**, *42*, 5642.

[47] D. Xiang, X. L. Wang, C. C. Jia, T. Lee, X. F. Guo, *Chem. Rev.* **2016**, *116*, 4318.
[48] C. C. Jia, B. J. Ma, N. Xin, X. F. Guo, *Acc. Chem. Res.* **2015**, *48*, 2565.
[49] Z. F. Liu, S. Wei, H. Yoon, O. Adak, I. Ponce, Y. Jiang, W. D. Jang, L. M. Campos, L. Venkataraman, J. B. Neaton, *Nano Lett.* **2014**, *14*, 5365.
[50] B. Kim, S. H. Choi, X. Y. Zhu, C. D. Frisbie, *J. Am. Chem. Soc.* **2011**, *133*, 19864.
[51] W. J. Cho, Y. Cho, S. K. Min, W. Y. Kim, K. S. Kim, *J. Am. Chem. Soc.* **2011**, *133*, 9364.
[52] R. J. Nichols, S. J. Higgins, *Acc. Chem. Res.* **2016**, *49*, 2640.
[53] X. F. Guo, J. P. Small, J. E. Klare, Y. L. Wang, M. S. Purewal, I. W. Tam, B. H. Hong, R. Caldwell, L. M. Huang, S. O'Brien, J. M. Yan, R. Breslow, S. J. Wind, J. Hone, P. Kim, C. Nuckolls, *Science* **2006**, *311*, 356.
[54] Y. Cao, S. Dong, S. Liu, L. He, L. Gan, X. Yu, M. L. Steigerwald, X. Wu, Z. Liu, X. Guo, *Angew. Chem., Int. Ed.* **2012**, *51*, 12228.
[55] H. M. Wen, W. G. Li, J. W. Chen, G. He, L. H. Li, M. A. Olson, A. C.-H. Sue, J. F. Stoddart, X. F. Guo, *Sci. Adv.* **2016**, *2*.
[56] C. C. Jia, A. Migliore, N. Xin, S. Y. Huang, J. Y. Wang, Q. Yang, S. P. Wang, H. L. Chen, D. M. Wang, B. Y. Feng, Z. R. Liu, G. Y. Zhang, D. H. Qu, H. Tian, M. A. Ratner, H. Q. Xu, A. Nitzan, X. F. Guo, *Science* **2016**, *352*, 1443.
[57] Y. A. Zhao, B. Ashcroft, P. M. Zhang, H. Liu, S. M. Sen, W. Song, J. Im, B. Gyarfas, S. Manna, S. Biswas, C. Borges, S. Lindsay, *Nat. Nanotechnol.* **2014**, *9*, 466.
[58] P. Pang, B. A. Ashcroft, W. S. Song, P. M. Zhang, S. Biswas, Q. Qing, J. L. Yang, R. J. Nemanich, J. W. Bai, J. T. Smith, K. Reuter, V. S. K. Balagurusamy, Y. Astier, G. Stolovitzky, S. Lindsay, *ACS Nano* **2014**, *8*, 11994.
[59] S. A. Chang, S. Huang, J. He, F. Liang, P. M. Zhang, S. Q. Li, X. Chen, O. Sankey, S. Lindsay, *Nano Lett.* **2010**, *10*, 1070.
[60] M. Tsutsui, M. Taniguchi, K. Yokota, T. Kawai, *Nat. Nanotechnol.* **2010**, *5*, 286.
[61] S. Huang, J. He, S. Chang, P. M. Zhang, F. Liang, S. Q. Li, M. Tuchband, A. Fuhrmann, R. Ros, S. Lindsay, *Nat. Nanotechnol.* **2010**, *5*, 868.
[62] X. G. Liang, S. Y. Chou, *Nano Lett.* **2008**, *8*, 1472.
[63] J. Lagerqvist, M. Zwolak, M. D. Ventra, *Nano Lett.* **2006**, *6*, 779.
[64] M. Tsutsui, S. Rahong, Y. Iizumi, T. Okazaki, M. Taniguchi, T. Kawai, *Sci. Rep.* **2011**, *1*, 46.
[65] P. S. Spinney, S. D. Collins, D. G. Howitt, R. L. Smith, *Nanotechnology* **2012**, *23*, 135501.
[66] T. Ohshiro, K. Matsubara, M. Tsutsui, M. Furuhashi, M. Taniguchi, T. Kawai, *Sci. Rep.* **2012**, *2*, 501.
[67] A. C. Aragones, N. L. Haworth, N. Darwish, S. Ciampi, N. J. Bloomfield, G. G. Wallace, I. Diez-Perez, M. L. Coote, *Nature* **2016**, *531*, 88.
[68] C. Nicolai, F. Sachs, *Biophys. Rev. Lett.* **2014**, *8*, 191.
[69] P. Gong, R. Levicky, *Proc. Natl. Acad. Sci. USA* **2008**, *105*, 5301.
[70] S. C. Kou, B. J. Cherayil, W. Min, B. P. English, X. S. Xie, *J. Phys. Chem. B* **2005**, *109*, 19068.
[71] W. Xu, J. S. Kong, P. Chen, *J. Phys. Chem. C* **2009**, *113*, 2393.
[72] J. B. Witkoskie, J. S. Cao, *J. Chem. Phys.* **2004**, *121*, 6361.
[73] H. P. Lu, L. Y. Xun, X. S. Xie, *Science* **1998**, *282*, 1877.
[74] T. Chen, Y. Zhang, W. Xu, *J. Am. Chem. Soc.* **2016**, *138*, 12414.

